View Article Online
View Journal

RSC Advances

Accepted Manuscript

This article can be cited before page numbers have been issued, to do this please use: W. Darwich, C. Gedig, H. SROUR, C. Santini and M. H. G. Prechtl, *RSC Adv.*, 2013, DOI: 10.1039/C3RA43909G.

This is an *Accepted Manuscript*, which has been through the RSC Publishing peer review process and has been accepted for publication.

Accepted Manuscripts are published online shortly after acceptance, which is prior to technical editing, formatting and proof reading. This free service from RSC Publishing allows authors to make their results available to the community, in citable form, before publication of the edited article. This *Accepted Manuscript* will be replaced by the edited and formatted *Advance Article* as soon as this is available.

To cite this manuscript please use its permanent Digital Object Identifier (DOI®), which is identical for all formats of publication.

More information about *Accepted Manuscripts* can be found in the **Information for Authors**.

Please note that technical editing may introduce minor changes to the text and/or graphics contained in the manuscript submitted by the author(s) which may alter content, and that the standard **Terms & Conditions** and the **ethical guidelines** that apply to the journal are still applicable. In no event shall the RSC be held responsible for any errors or omissions in these *Accepted Manuscript* manuscripts or any consequences arising from the use of any information contained in them.

RSCPublishing

www.rsc.org/advances
Registered Charity Number 207890

View Article Online
DOI: 10.1039/C3RA43909G

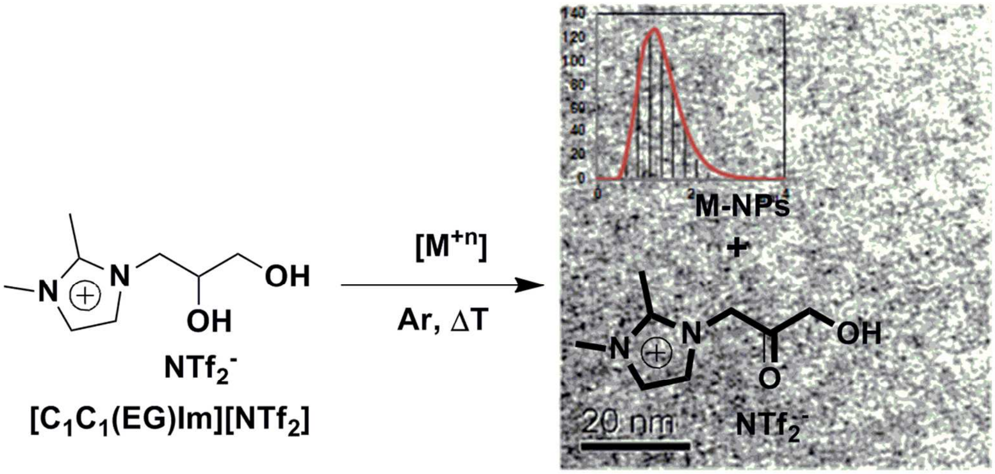

Graphical Abstract
112x53mm (300 x 300 DPI)

RSC Advances

Cite this: DOI: 10.1039/c0xx00000x

www.rsc.org/xxxxxx

Full Paper

Single step synthesis of metallic nanoparticles using dihydroxyl functionalized ionic liquids as reductive agent

Walid Darwich,[a] Christian Gedig,[b] Hassan Srour,[a] Catherine C. Santini,[a]* Martin H. G. Prechtl[b]*

Received (in XXX, XXX) 25th July 2013, Accepted Xth XXXXXXXXX 20XX

DOI: 10.1039/b000000x

In the last years, ionic liquids (ILs) have revealed their broad versatility for application towards the synthesis of shape and size controlled nanoscale metal catalysts, respectively metal(0) nanoparticles (M-NPs) in absence of additive ligand. ILs play the role of solvent and ligand. In our work, we depict the synthesis of M-NPs (M = Cu, Ag, Ni, Ru) using dihydroxyl functionalized imidazolium ILs 1-(2,3-dihydroxypropyl)-2,3-dimethylimidazolium bis(trifluoromethanesulfonimide) $[C_1C_1(EG)Im][NTf_2]$ as simultaneously solvent, stabilizer and reductive agent. In this IL the formation of stable dispersion of NPs from silver and copper salts in the absence of any reducing agent has been observed. The comparison of the ^{13}C-NMR, and IR data of pure IL and IL-NP (Cu and Ag) suspensions proved the oxidation of the hydroxyl group to a carbonyl group, confirming that the dihydroxyl function of the IL acted as the reducing agent. This oxido-reduction depends on the nature of metal. No reaction occurred with Ni^{II} and Ru^0 precursors, and with Ru^{II} and Ni^0 salts the formation of M-NPs is due to the activation of the acidic protons on the imidazolium ring. The Ru-NPs were then further evaluated for selective partial hydrogenation, here we observed good selectivities for α,β-unsaturated compounds such cyclohexenone and cinnamic aldehyde, which can be converted exclusively into the unsaturated alcohols or saturated alcohols.

Introduction

The progress in the comprehension of metallic nanoparticles (NPs) is a central aspect due to their great potential in the development of new and innovative materials for applications in areas such as catalysis or microelectronics.[1-11] Their small sizes, generally reported between 1 and 100 nm, lead to unique physico-chemical properties between the bulk and molecular states, which vary greatly with small changes in NP size. For example, the catalytic properties of NPs are largely determined by the energy of the surface atoms, in turn controlled by the number of neighbouring atoms, dictated by their size, as well as the presence and nature of ligands or supports.[12-16] Particles less than 10 nm in diameter are particularly interesting in catalysis, due to their high surface to volume ratio, and are also greatly influenced by the aforementioned size-effect.[17, 18] To prevent aggregation, NPs must be stabilized by the use of capping agents such as (water-soluble) polymers, quaternary ammonium salts, surfactants, ligands or polyoxoanions, providing electronic and/or steric protection.[19, 20] In this context, ionic liquids (ILs), defined as low temperature molten salts, have emerged as one of the most important and the most investigated media for the synthesis of metal NPs.[21-24] Moreover, an advantage of using ILs is that stabilizing additives such as ligands, polymers and supports are not required.[23] The soluble transition-metal NPs are *in situ* generated in ILs mainly from the following routes a) simple reduction of $M^{(n+)}$ salts, b) decomposition of the organometallic complexes in the formal zero oxidation state, c) bombardment of bulk metal precursors with deposition onto the ILs and d) phase transfer of pre-formed NPs in water or organic solvents to the IL (Scheme 1).[23]

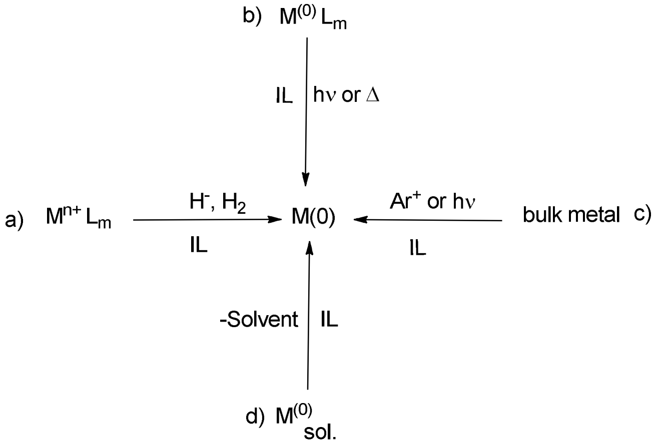

Scheme 1: General methods used to prepare metal NPs in ILs.

In general, appropriate metal complexes or metal salts are

View Article Online
DOI: 10.1039/C3RA43909G

dispersed / dissolved in the ILs and subsequently reduced to the corresponding M-NPs, in the ubiquitous presences such as molecular dihydrogen gas,[25] ethylene glycol,[26] ascorbic acid, [27] hydrazine,[28] and disulfide.[29] In some cases, the IL has been claimed to be the reducing agent.[30-32] However, in certain cases, an aqueous solution of ILs was used. For instance, the formation of Au^0 microprisms in 1-butyl-3-methylimidazolium hexafluorophosphate in the presence of water has been explained by an oxido-reduction reaction consuming the IL (Scheme 2) and yielding [Cl^-] anions in the media.

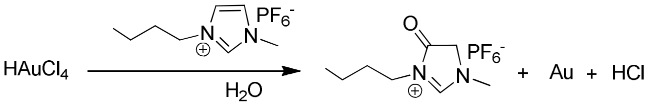

Scheme 2: The formation of Au^0 microprisms in 1-butyl-3-methylimidazolium hexafluorophosphate in the presence of water.[30]

In water, using halide salts of mono and di-hydroxyl ILs as surfactants, a suspension of narrow size Ag^0-NPs (means size 2 or 4 nm following the IL) stabilized by the hydroxyl groups has been obtained using $AgNO_3$ as metal source (Scheme 3).[31] The oxidation of the OH-group to the corresponding aldehyde during the reduction of Ag^I into Ag^0 has been evidenced by IR spectroscopy.

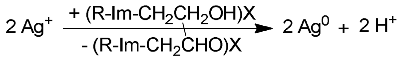

$$2\,Ag^+ \xrightarrow[-\,(R\text{-}Im\text{-}CH_2CHO)X]{+\,(R\text{-}Im\text{-}CH_2CH_2OH)X} 2\,Ag^0 + 2\,H^+$$

Scheme 3: Preparation of Ag NPs using the hydroxyl group linked to the imidazolium cation as reducing agents.[31]

Pointing out that the particle size control can also be influenced by dissolved halides, especially in aqueous solutions of ILs. For instance, [Cl^-] anions and water may coordinate onto the metal surface, acting as extra-stabilizers, but also influencing the nanoparticle properties (optical, magnetic and catalytic).[33]

Contrary, in our previous studies using neat anhydrous alkyl imidazolium IL like [C_1C_nImNTf$_2$] (n = 4 and 6) as reaction media under argon, the formation of Ru^0-NPs and Ni^0-NPs by reduction of bis(2-methylallyl)(1,5-cyclooctadiene) ruthenium [Ru^{II}(Me-allyl)$_2$(COD)], respectively auto-decomposition of bis(η^4-1,5-cyclooctadiene)nickel [Ni^0(COD)$_2$] have been observed.[32] These methods afforded small-sized and mono-dispersed Ru-NPs (1-3 nm; mean diameter: 2.0±0.3 nm) and for Ni-NPs a broader size distribution (2-12 nm; mean diameter: 7.0±2.0 nm and higher agglomeration.

Generally, the NP formation in solution depends on three key factors (i) the solvent medium, (ii) the reducing agent, and (iii) the stabilizer. ILs are largely depicted as solvent and stabilizer for NPs and are scarcely used as a reducing agent. In this work, we report, that an anhydrous dihydroxyl functionalized imidazolium IL, namely 1-(2,3-dihydroxypropyl)-2,3-dimethylimidazolium bis(trifluoromethanesulfonimide ([C_1C_1(EG)Im][NTf_2]) based on a building block derived from abundant biomass namely glycerine, conjuncts these three roles: solvent, stabilizer, surface modifier and reductant in the *in situ* synthesis of NPs.

The role as metal nanoparticle surface modifier we have investigated in particular regarding the partial hydrogenation of organic substrates with ruthenium nanoparticles. In previous works we reported that functional groups in the moieties of ionic liquid side-chain show significant influence towards the selectivity while using Ru-NPs as hydrogenation catalyst for arene versus nitrile entities**.** [38-39] There, we showed that nitriles completely suppress the usual occurring arene hydrogenation.

Results and Discussion

In order to prove the specific reactivity of [C_1C_1(EG)Im][NTf_2], the thermal stability of all chosen metal precursors (Table 1) in this IL under argon have also been studied in [C_1C_4Im][NTf_2]. Each precursor has been successively heated in IL under argon until a colour change was observed (Scheme 4).

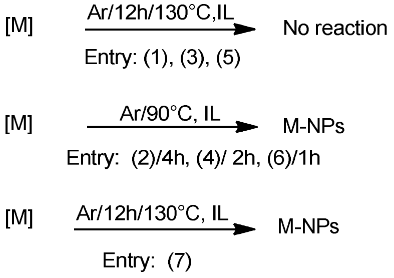

$$[M] \xrightarrow[\text{Entry: (1), (3), (5)}]{\text{Ar/12h/130°C,IL}} \text{No reaction}$$

$$[M] \xrightarrow[\text{Entry: (2)/4h, (4)/ 2h, (6)/1h}]{\text{Ar/90°C, IL}} \text{M-NPs}$$

$$[M] \xrightarrow[\text{Entry: (7)}]{\text{Ar/12h/130°C, IL}} \text{M-NPs}$$

Scheme 4: General overview for the decomposition/reduction of metal precursors in [C_1C_1(EG)Im][NTf_2] at the applied reaction temperatures and durations (refer Table 1)

Experiments with $AgNO_3$, CuMes, anhydrous $CuSO_4$ and Ru(COD)(COT) in [C_1C_4Im][NTf_2] showed no reaction. In contrast Ru(Me-allyl)$_2$(COD) and Ni(COD)$_2$ already decompose at low temperature.[32] In [C_1C_1(EG)Im][NTf_2] no reactions were observed with anhydrous $CuSO_4$, Ru(COD)(COT) and Ni(NTf_2)$_2$ after stirring overnight at 130 °C, neither colour changes of the solutions were visible, nor NPs could be located in TEM images (Table 1, Entries 1, 3, 5). In [C_1C_1(EG)Im][NTf_2], Ru(Me-allyl)$_2$(COD), Ni(COD)$_2$ and $AgNO_3$ led to NPs at 90 °C in 1, 2 and 4 h, respectively (Table 1, Entries 2, 4, 6). The formation of Cu-NPs in [C_1C_1(EG)Im][NTf_2] from mesityl copper (CuMes) was observed after 12 h at 130 °C (Table 1, Entry 7). All results with the corresponding mean diameters are listed in Table 1.

Table 1: Experimental conditions and the mean sizes of the M-NPs formed in [C_1C_1(EG)Im][NTf_2] under argon

Entry	Metal Source [M][a]	t[h]/T[°C]	NP size (nm)
1	$CuSO_4$	12 h/130 °C	n.r*
2	$AgNO_3$	4 h/90 °C	4.7± 0.8nm
3	Ru(COD)(COT)	12 h/130 °C	n.r*
4	Ni(COD)$_2$	2 h/90 °C	3.5 ± 0.5nm
5	Ni(NTf_2)$_2$	12 h/130 °C	n.r*
6	Ru(COD)(Me-allyl)$_2$	1 h/90 °C	6.9 ± 1.3nm
7	CuMes	12 h/130 °C	5.7 ± 0.8nm

[a][C] 0.01 M of metal precursor in 1.5 ml of [C_1C_1(EG)Im][NTf_2], n.r*= no reaction.

View Article Online
DOI: 10.1039/C3RA43909G

Silver Nanoparticle Synthesis:

Silver nitrate is reduced in aqueous mono- and dihydroxyl functionalized imidazolium ionic liquid within in 2 h at 60°C, the generated Ag-NPs show sizes of 4-8 nm and 2-4 nm, respectively.[31] The presence of dihydroxyl functional group induces probably a higher size control. In our experimental conditions, (Table 1, Entry 2: 2 h at 90 °C in neat $[C_1C_1(EG)Im][NTf_2]$) the Ag-NP were formed with a mean size about 4.7 ± 0.8nm (Figure 1) for 90% of the NP population and at ca. 10 nm for 10 %. The structure of individual particles was investigated using HRTEM, Figure 1. The interplanar distance measured from this micrograph is 0.2295nm (table 2), corresponding to the (101) interplanar distance of hexagonal metallic Ag.

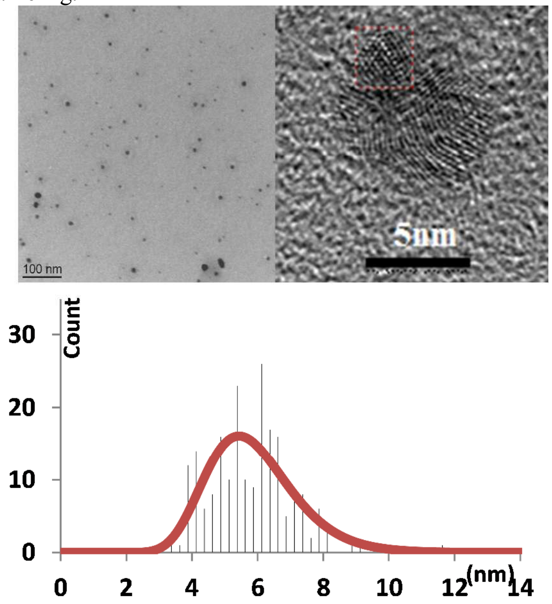

Figure 1: TEM and HRTEM images of Ag-NPs in $[C_1C_1(EG)Im][NTf_2]$ and their particles size distribution

Table 2 : Theorical[‡] (JCPD 04-016-1388) and experimental interplanar distances (nm), and angles° for AgNPs

spot	hkl	d(exp) nm	d(theo) nm	Angle (exp)	Angle (theo)
1	101	0.2295	0.224270	0	0
2	011	0.2466	0.224270	50.29	52.44
3	-110	0.2529	0.224270	119.67	116.22

FT-IR spectroscopy was used to investigate the interactions between different species and changes in chemical composition of the mixtures. Figure 2 shows the FT-IR spectra of pure $[C_1C_1(EG)Im][NTf_2]$ (b), and of the reaction media after the formation of Ag-NPs (a). In the IR spectra of the neat $[C_1C_1(EG)Im][NTf_2]$, a broad peak of (3220-3720) cm^{-1} centred at 3504 cm^{-1} and peaks at 1530 cm^{-1} and 1590 cm^{-1} are related to the hydroxyl function. In the IR spectra of the Ag-NP suspensions, all these bands are less wide and changed from (3220-3720 cm^{-1}) to (3500-3600 cm^{-1}) and are centred at 3525 cm^{-1} and a new peak is observed at 1645 cm^{-1} assigned to the vibration of conjugated carbonyl groups resulting from the oxidation of the OH-group, during the reduction of metal ions (Figure 2 and Scheme 5). The formation of this carbonyl function is also confirmed by the peak at 205 ppm assigned to a $\delta_{C=O}$ in the ^{13}C NMR spectra of the Ag-NP suspension (Figure 3).

Copper Nanoparticle Synthesis:

The decomposition of mesityl-copper (CuMes) in $[C_1C_1(EG)Im][NTf_2]$ at 130 °C within 12 h yielded well dispersed Cu-NPs with a mean size around 5.7 nm (Figure 4). While, CuMes in $[C_1C_4Im][NTf_2]$ under 0.9 MPa of H_2 resulted in Cu-NPs with a size distribution centred around 6.4 nm at 30 °C, respectively 4.5 nm at 100 °C reaction temperatures.[4]

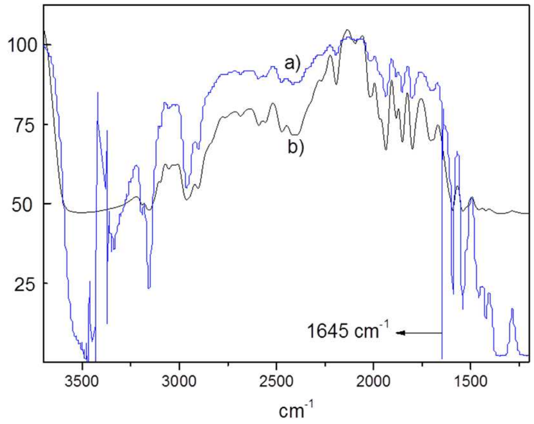

Figure 2 FT-IR spectra of suspension of (a) Ag-NPs in $[C_1C_1(EG)Im][NTf_2]$ after reaction (b) pure $[C_1C_1(EG)Im][NTf_2]$

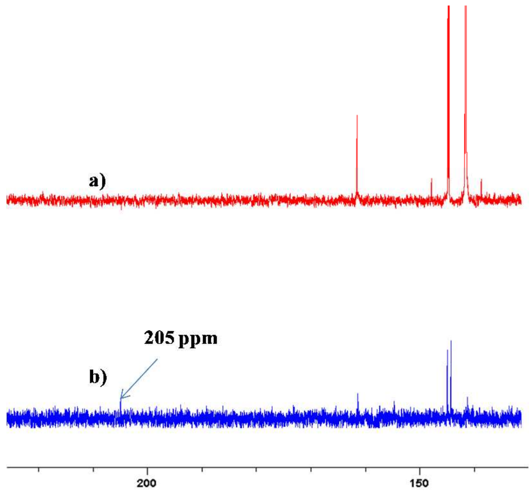

Figure 3: ^{13}C NMR spectra a)pure $[C_1C_1(EG)Im][NTf_2]$; b) suspension of Ag-NPs in $[C_1C_1(EG)Im][NTf_2]$

Note that no reaction occurs with $CuSO_4$ in $[C_1C_1(EG)Im][NTf_2]$ whatever the experimental conditions are. Contrarily, Cu-NPs are formed using this salt in $C_1C_4ImBF_4$ in the presence of hydrazine as a reducing agent and ethylene glycol playing the role as ligand.[28] The comparison of the FT-IR spectra of the Cu-NP suspension in $[C_1C_1(EG)Im][NTf_2]$ (Figure S1a) and the pure $[C_1C_1(EG)Im][NTf_2]$ (Figure S1b) shows the presence of stretching peaks at 1645 cm^{-1} corresponding to a carbonyl group vibration, similar to the Ag-NPs synthesis (see above).

With $AgNO_3$ and CuMes an oxidation of one of the hydroxyl to carbonyl function was observed affording Ag-NPs and Cu-NPs, following the oxido-reduction mechanism depicted in Scheme 5.

View Article Online
DOI: 10.1039/C3RA43909G

The interplanar distance measured from this micrograph is 0.2012 nm (table 3), which coincides with the (1 1 1) interplanar distance of cubic metallic Cu.

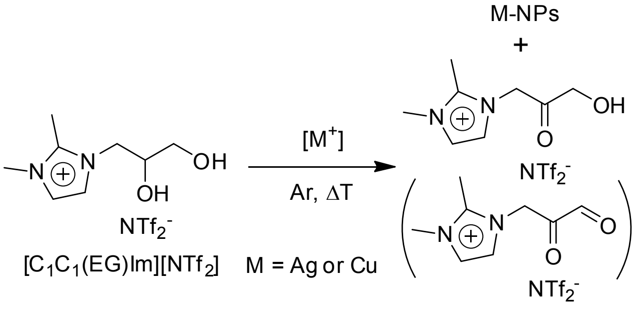

Scheme 5: Proposed oxido-reduction mechanism

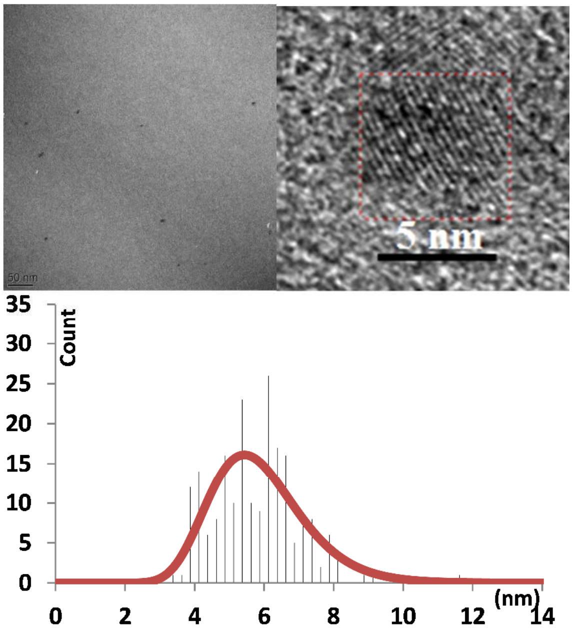

Figure 4 : TEM and HRTEM images of Cu-NPs in [C$_1$C$_1$(EG)Im][NTf$_2$] and their particles size distribution

Table 3 : Theoretical‡ (JCPD 04-001-3342) and experimental interplanar distances (nm) and angles of CuNPs

spot	hkl	d(exp) nm	d(theo) nm	Angle (exp)	Angle(theo)
1	1 1 1	0.2012	0.2087240	0	0
2	2 0 0	0.1753	0.1807600	90.11	90
3	2 2 0	0.1344	0.1278170	42.90	45

Nickel Nanoparticle Synthesis:

An auto-decomposition of the organometallic complex Ni(COD)$_2$ is observed affording nickel nanoparticles NiNPs in neat [C$_1$C$_4$Im][NTf$_2$] at room temperature under argon. This occurs via a C-H insertion at the acidic C$_2$-position of the imidazolium ring and the formation of N-heterocyclic carbenes.[32] To overcome this side reaction, we have used [C$_1$C$_1$(EG)Im][NTf$_2$] substituted with a methyl group at the C$_2$-position. When Ni(COD)$_2$ was dissolved in [C$_1$C$_1$(EG)Im][NTf$_2$] under argon, no reaction was observed at room temperature. At 90 °C after 2 h, a homogeneous suspension of Ni-NPs was obtained with a narrow size distribution centred around 3.5 ± 0.5nm (Figure 5).

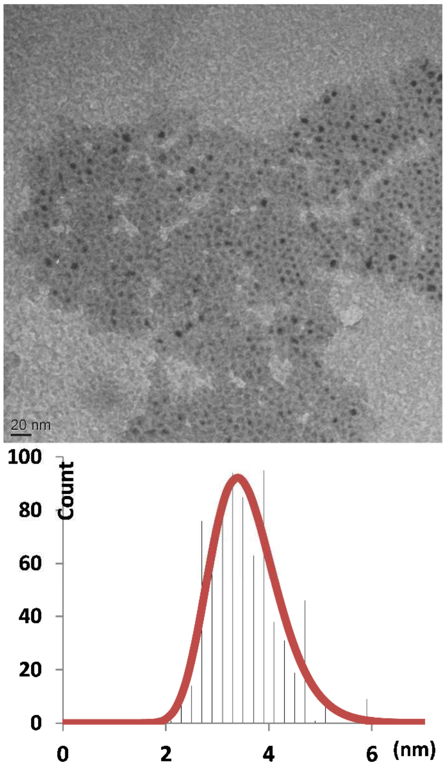

Figure 5 : TEM image of Ni-NPs in [C$_1$C$_1$(EG)Im][NTf$_2$] and particles size distribution

The analysis of the resulting solution by gas chromatography showed as major product cycloocta-1,5-diene (1,5-COD), accompanied by its isomer cycloocta-1,3-diene (1,3-COD) and cyclooctene and traces of cyclooctane (Figure S2). The presence of large amount of 1,5-COD could be explained by a ligand exchange with a diol functionality. Following Route A (Scheme 6), the formation of Ni^{II}-H is necessary to explain the isomerization of 1,5-COD into 1,3-COD. But, Ni^{II} salt are not reduced to Ni-NPs, in this media, *vide supra,* thus Route A (Scheme 6) could not explain the experimental results. Consequently the decomposition can only be explained by C-H insertion at the less acidic C$_4$-H, C$_5$-H positions of the imidazolium ring and generation of transitory non-classical NHC ligands; Route B in Scheme 6.[32, 34]

Ruthenium Nanoparticle Synthesis:

While Ru(COD)(COT) under H$_2$ since 0 °C readily affords Ru-NPs in any ILs; contrarily, in [C$_1$C$_1$(EG)Im][NTf$_2$] under argon, as well in [C$_1$C$_4$Im][NTf$_2$] no Ru-NPs are observed.
In [C$_1$C$_4$Im][NTf$_2$], Ru(Me-allyl)$_2$(COD) is readily decomposed at room temperature after prolonged reaction time (Scheme S1).[32]
In [C$_1$C$_1$(EG)Im][NTf$_2$], Ru-NPs were formed at 90°C after 1h,

View Article Online
DOI: 10.1039/C3RA43909G

leading to a broader size distribution (6.9 ± 1.3 nm; Figure 6; Figure S3). These NP could result from a decomposition as already reported,[32] through an oxido-reductive reaction as observed with Cu and Ag precursors or by the attack on the two acidic protons C_4-H, C_5-H as observed with $Ni(COD)_2$. No difference was observed between the FT-IR and ^{13}C NMR spectra of the media before and after reaction (Figure S4).

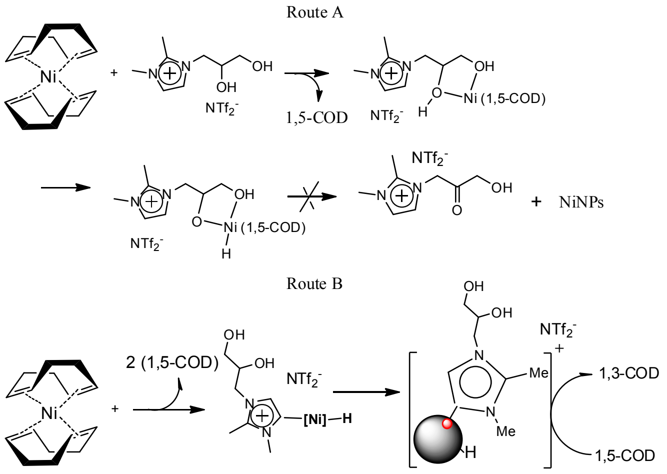

Scheme 6 : Possible mechanism to explain the formation of Ni-NPs in [C1C1(EG)Im][NTf2].[32]

The gas chromatogram of the reaction media was similar to the one obtained with $Ni(COD)_2$ (Figure S5) due to ligand loss. Consequently, as for $[Ni(COD)_2]$, the formation of M-NPs from $[Ru(COD)(2\text{-methylallyl})_2]$, was probably due to the activation of the acidic protons on the imidazolium ring.[32] However, in $[C_1C_1(EG)Im][NTf_2]$, the formation Ru-NPs differs to those previously reported in non-functionalized ILs such as $[C_1C_4Im][NTf_2]$ because contrary in $[C_1C_1(EG)Im][NTf_2]$ no imidazolium ring fragmentation was observed during the reaction of the ruthenium precursor with the IL.[32]

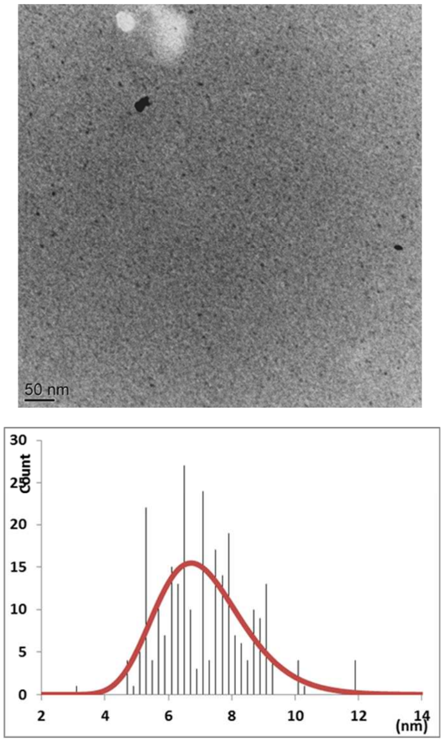

Figure 6 : TEM image of Ag-NPs in $[C_1C_1(EG)Im][NTf_2]$ and particles size distribution

Catalytic Hydrogenation with Ruthenium Nanoparticles:

For further evaluation of the properties of the ruthenium nanoparticles we tested their catalytic activity for hydrogenation of different unsaturated substrates with arene, carbonyl and alkene functionalities (Table 4). Moreover, recycling experiments were performed for two aromatic substrates (Figure 7).

For the study of nanoscale catalysts, one important factor is the surface to volume ratio of the particles. Of course one cannot exclude partial aggregation of the nanoparticles, and even topology changes,[23] but the metal atoms located on the surface are accessible to interact with substrates, hence are potentially catalytically active. For the calculation of the amount of surface atoms on a nanoparticle, we estimated the volume of a spherical particle with a mean diameter of 6.9 nm. This diameter corresponds to a particle volume of 172.0 nm^3 consisting of approx. 11862 atoms. According to the magic numbers methodology as convenient tool for the evaluation of cluster formation,[35-37] the number of shells is 16 and this corresponds to ~18 % surface atoms which are potentially active for heterogeneous catalysed reactions such as arene hydrogenation. The surface to volume ratio was used to determine the substrate catalyst ratio and TONs for the hydrogenation reactions. The Ru-NPs dispersions in ILs are stable in presence of other solvents. Therefore these IL-phases are interesting for their application in multiphase catalysis.

The hydrogenation of toluene (Table 4; Entry 1-2) only occurred at higher pressure. This stays in contrast to previous studies with unfunctionalised ILs like $[C_1C_4Im][NTf_2]$ where hydrogenation already occurred in high conversions at H_2 pressures as low as 4 bar.[32, 38] This observation can be related to two properties of this

View Article Online
DOI: 10.1039/C3RA43909G

IL: (I) The gas solubility depends on the viscosity of the IL, as $[C_1C_1(EG)Im][NTf_2]$ is a highly viscous material, higher pressures are necessary to guarantee significant amounts in the IL-phase of dissolved hydrogen. (II) Functional groups linked to the IL may act as ligands on the metal surface, and these ligands may hinder the coordination of the substrate, thus suppressing the hydrogenation of arenes, but still allowing the hydrogenation of functional groups via ligand-exchange on the surface.[39] At higher pressure (40 bars) toluene was completely converted into methylcyclohexane in five runs with a total TON of >>2600, this proves the capability for recycling without significant loss of activity (Entry 2).

Table 4: Hydrogenation of different substrates with RuNPs.

Entry	Substrate^a	t [h]	p (bar)^a	conv. [%]^b	TON	product selectivity^b
1	toluene **1**	24	4	0	0	-
2	toluene **1**	24	40	>99	2640^e	-
3	acetophenone **2**	24	15	91^d	1847^e	50:50^d (**6**:**7**)
4	cinnamic aldehyde **5**	24	15	>99	438	100 (**8**)
5	cinnamic aldehyde **5**	4	15	56	245	100 (**9**)
6	cyclohexene **3**	20	15	>99	550	-
7	cyclohexen-2-one **4**	24	15	>99	572	100 (**10**)
8	cyclohexen-2-one **4**	3	15	>99	572	100 (**11**)

^{a} 1 mL (7.9-10.3 mmol); reaction temp. = 75 °C; ^{b} determined by ^{1}H-NMR. ^{c} in all five runs. ^{d}first run. ^{e}total TON of 5 (toluene) or 4 (acetophenone) runs. 1,1-phenylethanol **6**; 1,1-cyclohexylethanol **7**; 3-phenylpropanol **8**, 3-phenylpropanal **9**, cyclohexanol **10**, cyclohexanone **11**

For proving the chemo-selectivity of the catalyst phase, hence to distinguish between a suppressed hydrogenation due to gas solubility/IL-viscosity or ligand-like poisoning of the surface (see above), we used acetophenone **2** as model substrate (Table 4; Entry 3). Here, we obtained a mixture of 1-phenylethanol **6** and 1-cyclohexylethanol **7** in a ~1:1 ratio after 24 h in high conversions (91 %; Entry 3). This ratio undergoes a variation in four subsequent runs during the recycling of the catalyst phase (Figure 7).

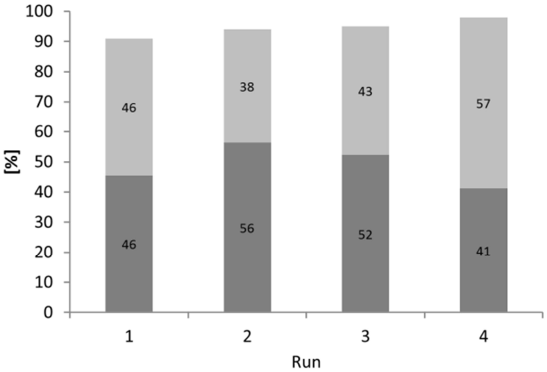

Figure 7: Hydrogenation of acetophenone **2** in recycling runs, yielding 1-phenylethanol **8** (dark grey) and 1-cyclohexylethanol **9** (light grey)

However, one could say that there is no significant chemo-selectivity for the hydrogenation of the arene moiety and the ketone. This implies that in this certain case there is no blocking of the catalyst surface by the diol of $[C_1C_1(EG)Im][NTf_2]$ as surface ligand.[39] Indeed, the intermediate 1-phenylethanol **8** can still coordinate as O-ligand onto the surface via ligand exchange (substrate vs. IL) which also brings the arene moiety close to the surface, hence accessible for hydrogenation (Table 4, Entry 3; Figure 8). Interestingly and contrary, the hydrogenation of cinnamic aldehyde gives under similar conditions selectively 3-phenylpropanol at high conversions (Entry 4; >99%), respectively 3-phenylpropanal **9** at moderate conversions (Entry 5; 56%). The aldehyde and olefin are hydrogenated subsequently and can be kinetically distinguished, but the arene remains untouched. This is again most likely due to steric aspects. During the coordination onto the surface via the oxygen, the propyl-chain acts as a spacer and the arene moiety is not accessible for hydrogenation (Figure 9). Furthermore, we tried then to distinguish between an olefin and ketone in a hydrogenation. The hydrogenation of cyclohexene gave also quantitative conversion within one hour (Table 4; Entry 6). Following, we used cyclohexen-2-one **4** which is also selectively converted into cyclohexanol **10** in high conversions (Table 2; Entry 7; >99%) and at shorter reaction times cyclohexanone **11** is formed exclusively. Again both double bonds can be hydrogenated, similar to Entry 4, and a kinetic distinction is possible with high selectivity for the partially and fully hydrogenated products. This shows that the tested catalytic system hydrogenate olefins and aldehydes/ketones with kinetic selectivity. Arene hydrogenation occurs effectively in absence of functional groups (Entry 1-2), but it is slightly hindered already in presence of a neighbouring functional group (Entry 3), and it can be fully blocked while incorporating a functional group via a spacer (Entry 4) leading to a suppression of the arene coordination, hence, the arene moiety is not accessible for hydrogenation.

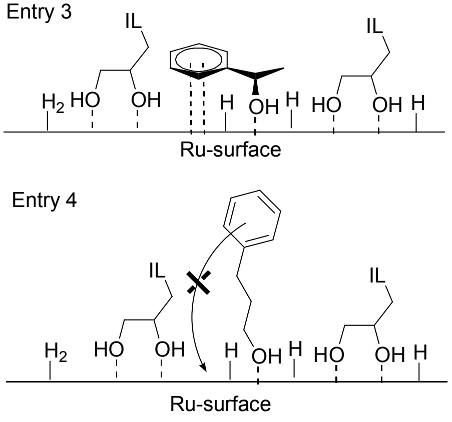

Figure 8: Model for the coordination of intermediates/products during the hydrogenation in presence of $[C_1C_1(EG)Im][NTf_2]$.

Experimental

All operations were performed in the strict absence of oxygen and water under a purified argon atmosphere using glovebox (Jacomex or MBraun) or vacuum-line techniques if not otherwise indicated. *Materials:* Mesitylcopper Cu-Mes (Nanomeps, 97%), Bis(η^3-2-methylallyl)(η^4-1,5-cyclooctadiene)ruthenium Ru(Me-allyl)$_2$(COD) (Strem, 97%), bis(η^4-1,5-cyclooctadiene) nickel $Ni(COD)_2$ (Strem) , bis(trifluoromethylsulphonyl)nickel $Ni(NTf_2)_2$ (Solvionic), Silver nitrate ($AgNO_3$) (ACS reagent, ≥99.0%) and Copper sulfate ($CuSO_4$) (Sigma-Aldrich) were used without further purification. (η^4-1,5-cyclooctadiene)(η^6-1,3,5-

View Article Online
DOI: 10.1039/C3RA43909G

cyclooctatriene) ruthenium(0) Ru(COD)(COT), 1-butyl-3-methylimidazolium bis(trifluoromethane -sulfonimide), $[C_1C_4Im][NTf_2]$ and 1-(2,3-dihydroxypropyl)-2,3-dimethylimidazolium bis(trifluoromethanesulfonimide), $[C_1C_1(EG)Im][NTf_2]$ have been prepared as described in literature.[40-42]

General procedure for the nanoparticle synthesis:

In 1.5ml of $[C_1C_4Im][NTf_2]$ or $[C_1C_1(EG)Im][NTf_2]$ with a concentration of 0.01 M metallic salt or organometallic precursor were mixed, then the reaction media was kept under stirring overnight. At this step if no NP formation occurred, the temperature was maintained, until a colour change appeared, successively 2 h at 90 °C, then 4 h at 110 °C, and finally 130 °C for 12 h under argon atmosphere. No reaction was claimed, when after overnight at 130 °C, no colour change and no NPs in TEM images were observed. The reaction time and the results of these experiments are depicted in Table 1.

General procedure for the hydrogenation reactions:

1 mL of an unsaturated substrate (see Table 2) was added to ruthenium nanoparticles in $[C_1C_1(EG)Im][NTf_2]$ (see above; 1 mL IL) on air in a screw-capped vial with a septa and needle. The vial was placed in a stainless reactor and heated to 75 °C and pressurised with hydrogen (pressure see Table 2). After the indicated reaction time (Table 2), the autoclave was cooled to room temperature, the pressure was carefully released and an aliquot was analysed by ^{1}H-NMR in C_6D_6.

For the recycling, the IL-layer was extracted with pentane or ether (at least three times), the catalyst-/IL-phase was dried under reduced pressure and then the pure catalyst-/IL-phase was charged with substrate again.

Characterization:

The UV-Vis absorption spectra of the NP dispersions were recorded on a Unicowfz UV-2000 spectrophotometer. The Cu-, Ni-, Ru- and Ag-Np sizes were determined by transmission electron microscopy (TEM) on a Philips CM120 (120 keV), and the structure of the nanoparticles were examined using a Jeol-2010 transmission electron microscope (TEM) operated at a 200 KV acceleration voltage. TEM and HRTEM samples were prepared by dropping the IL solution onto a copper TEM grid with amphorous carbon over layers, followed by the removal of excess amounts of solution with filter paper. The preparation is stored in pill-box filled with argon and taken from the glove box only right before the analysis. ^{1}H- and ^{13}C-NMR spectra were recorded on a 300 MHz Bruker, with C_6D_6, CD_2Cl_2 or d_6-DMSO as external reference.

Conclusions

In unfunctionalized $C_1C_4ImNTf_2$ no formation of NP was observed under heating in absence of a reductive agent with Ag^INO_3, $Cu^{II}SO_4$, Cu^IMes , $Ni^{II}(NTf_2)_2$, and Ru^0(COD)(COT). In the dihydroxyl IL $C_1C_1(EG)ImNTf_2$ the synthesis of MNPs (M = Cu, Ag,) from Ag^INO_3 and Cu^IMes occurred through the oxidation of hydroxyl functionality. With $Ni^0(COD)_2$ and $[Ru^{II}(COD)(2\text{-methylallyl})_2]$, Ni-NPs and Ru-NPs were formed due to the activation of the acidic protons on the imidazolium ring. For all these *in situ* NP syntheses the $[C_1C_1(EG)Im][NTf_2]$ is simultaneously solvent, stabilizer and reductive agent. The catalytic hydrogenation with Ru nanoparticles in $[C_1C_1(EG)Im][NTf_2]$ showed that it is possible to hydrogenate effectively arenes only in absence of functional groups. And, the arene hydrogenation is completely blocked by incorporation of a functional group via a spacer. In this case only alkenes and aldehydes are accessible for hydrogenation via a ligand exchange reaction. Pointing out, that hydrogenation of alkenes is possible while aldehydes and ketones remain untouched

Acknowledgment

We acknowledge the Ministerium für Innovation, Wissenschaft und Forschung NRW (MIWF-NRW) for financial support within the Energy Research Program for the Scientist Returnee Award (NRW-Rückkehrerprogramm) for Dr M. H. G. Prechtl. Moreover, C. Gedig is thankful for helpful discussions with Sebastian Sahler and Michael T. Keßler. The HRTEM images were carried out by Dr.Philippe Arquillière to whom we are thankful.

Notes and references

[a] *Université de Lyon, Institut de Chimie de Lyon, UMR 5265 CNRS-Université de Lyon 1-ESCPE Lyon, LC2P2, Equipe Chimie Organométallique de Surface, ESCPE 43 Boulevard du 11 Novembre 1918, F-69616 Villeurbanne, France. Fax: 33(0)472431795; Tel: 33(0)472431810; catherine.santini@univ-lyon1.fr*

[b] *University of Cologne, Institute of Inorganic Chemistry - Research Group Catalysis, Greinstr. 6, D-50939 Köln, Germany. Fax: +49 -221-470-1788; Tel: +49 -221-470-1981; martin.prechtl@uni-koeln.de (corresponding)*

† Electronic Supplementary Information (ESI) available: For additional spectral data. See DOI: 10.1039/b000000x/

‡ M. I. Novgorodova,, A. Gorshkov and A. V. Mokhov, *Zap. Vses. Mineral. O-va*, 1979, **108**, 552-563; H. Brodowsky, A. Fruma, H. Sagunski and H. J. Schaller, *Z. Metallkd.* , 1982, **73**, 354 for the crystallographic data.

1. D. Astruc, F. Lu and J. R. Aranzaes, *Angew Chem Int Edit*, 2005, **44**, 7852-7872.
2. J. D. Scholten, B. C. Leal and J. Dupont, *Acs Catal*, 2012, **2**, 184-200.
3. M. H. G. Prechtl, J. D. Scholten and J. Dupont, *Molecules*, 2010, **15**, 3441-3461.
4. P. Arquilliere, P. H. Haumesser and C. C. Santini, *Microelectron. Eng.*, 2012, **92**, 149-151.
5. A. Umer, S. Naveed, N. Ramzan and M. S. Rafique, *Nano*, 2012, **7**.
6. F. Y. Cheng and J. Chen, *Chem Soc Rev*, 2012, **41**, 2172-2192.
7. P. Lignier, R. Bellabarba and R. P. Tooze, *Chem Soc Rev*, 2012, **41**, 1708-1720.
8. D. S. Wang and Y. D. Li, *Adv Mater*, 2011, **23**, 1044-1060.
9. S. Magdassi, M. Grouchko and A. Kamyshny, *Materials*, 2010, **3**, 4626-4638.
10. G. Konstantatos and E. H. Sargent, *Nat Nanotechnol*, 2010, **5**, 391-400.
11. R. Venkatesan, M. H. G. Prechtl, J. D. Scholten, R. P. Pezzi, G. Machado and J. Dupont, *J Mater Chem*, 2011, **21**, 3030-3036.
12. M. Valden, X. Lai and D. W. Goodman, *Science*, 1998, **281**, 1647.
13. A. T. Bell, *Science*, 2003, **299**, 1688 –1691.
14. G. Schmid, *Nanoparticles: From Theory to Application*, Wiley-VCH, Weinheim, 2004.
15. G. A. Somorjai and J. Y. Park, *Top Catal.*, 2008, **49**, 126-135.

View Article Online
DOI: 10.1039/C3RA43909G

16. D. Astruc, *Nanoparticles and Catalysis*, Wiley-VCH, Weinheim, 2008.
17. H. Boennemann, K. S. Nagabhushana and in *Metal Nanoclusters in Catalysis and Materials Science: The Issue of Size Control* ed. B. Corain, Schmid, G., Toshima, N., , Elsevier B.V, Amsterdam, 2008, pp. 21-48.
18. S. H. Joo, J. Y. Park, J. R. Renzas, D. R. Butcher, W. Y. Huang and G. A. Somorjai, *NANO LETTERS* 2010, **10**, 2709-2713
19. B. Chaudret, *Topics Organometal. Chem.*, 2005, **16**, 233-259.
20. B. Chaudret and K. Philippot, *Oil Gas Sci. Technol*, 2007, **62**, 799-817.
21. T. Welton, *Chem. Rev.*, 1999, **99**, 2071-2083.
22. P. Wasserscheid and T. Welton, *Ionic liquids in synthesis*, Wiley-VCH, Weinheim, 2008.
23. J. Dupont and J. D. Scholten, *Chem. Soc. Rev.*, 2010, **39**, 1780-1804.
24. J. P. Hallett and T. Welton, *Chem. Rev.*, 2011, **111**, 3508-3576.
25. J. Dupont, G. S. Fonseca, A. P. Umpierre, P. F. P. Fichtner and S. R. Teixeira, *J. Am. Chem. Soc.*, 2002, **124**, 4228-4229.
26. T. Y. Kim, W. J. Kim, S. H. Hong, J. E. Kim and K. S. Suh, *Angew. Chem., Int. Ed.*, 2009, **48**, 3806–3809.
27. H. J. Ryu, L. Sanchez, H. A. Keul, A. Raj and M. R. Bockstaller, *Angew. Chem. Int. Ed.*, 2008, **47**, 7639-7643.
28. M. Dewan, A. Kumar, A. Saxena, A. De and S. Mozumdar, *PLoS One*, 2012, **7**, e29131.
29. L. Zhao, C. Y. Zhang, L. Zhuo, Y. G. Zhang and J. Y. Ying, *J. Am. Chem. Soc.*, 2008, **130**, 12586-12587.
30. Y. Gao, A. Voigt, M. Zhou and K. Sundmacher, *Eur. J. Inorg. Chem.*, 2008, 3769-3775.
31. D. Dorjnamjin, M. Ariunaa and Y. K. Shim, *International Journal of Molecular Sciences*, 2008, **9**, 807-820.
32. M. H. G. Prechtl, P. S. Campbell, J. D. Scholten, G. B. Fraser, G. Machado, C. C. Santini, J. Dupont and Y. Chauvin, *Nanoscale*, 2010, **2**, 2601-2606.
33. L. L. Lazarus, C. T. Riche, N. Malmstadt and R. L. Brutchey, *Langmuir*, 2012, **28**, 15987-15993.
34. S. Gruendemann, A. Kovacevic, M. Albrecht, J. W. Faller Robert and H. Crabtree, *Chem. Commun.*, 2001, 2274-2275.
35. A. P. Umpierre, E. de Jesus and J. Dupont, *Chemcatchem*, 2011, **3**, 1413-1418.
36. K. S. Weddle, J. D. Aiken and R. G. Finke, *J Am Chem Soc*, 1998, **120**, 5653-5666.
37. B. K. Teo and N. J. A. Sloane, *Inorg Chem*, 1985, **24**, 4545-4558.
38. M. H. G. Prechtl, M. Scariot, J. D. Scholten, G. Machado, S. R. Teixeira and J. Dupont, *Inorg Chem*, 2008, **47**, 8995-9001.
39. M. H. G. Prechtl, J. D. Scholten and J. Dupont, *J Mol Catal a-Chem*, 2009, **313**, 74-78.
40. P. Pertici, G. Vitulli, M. Paci and L. Porri, *Dalton Trans.*, 1980, 1961-1964.
41. L. Magna, Y. Chauvin, G. P. Niccolai and J.-M. Basset, *Organometallics*, 2003, **22**, 4418-4425.
42. A. L. Lafarate, J. E. Bara, D. L. Gin and R. D. Noble, *Ind. Eng. Chem. Res.*, 2009, **48**, 8757-8756.